Available online at www.sciencedirect.com

SCIENCE DIRECT®

Journal of Petroleum Science and Engineering 48 (2005) 209–226

JOURNAL OF PETROLEUM SCIENCE & ENGINEERING

www.elsevier.com/locate/petrol

Geochemical characteristics and origin of natural gas and thermochemical sulphate reduction in Ordovician carbonates in the Ordos Basin, China

Chunfang Cai[a,*], Guoyi Hu[b], Hong He[c], Jian Li[b], Jianfeng Li[d], Yasheng Wu[a]

[a]*Key Laboratory of Mineral Resources, Institute of Geology and Geophysics, CAS, P.O. Box 9825, Qijiahuozi, Chaoyang district, Beijing 100029, PR China*

[b]*Langfang Branch of Petroleum Exploration and Development Institute, PetroChina, Lanfang, Hebei Province, 065007, PR China*

[c]*Exploration & Production Research Institute, SINOPEC, Beijing, 100083, PR China*

[d]*Research Institute of Exploration and Development, Changqing Oil and Gas Field Company, PetroChina, Xi'an, Shanxi Province, PR China*

Received 13 January 2005; received in revised form 17 June 2005; accepted 20 June 2005

Abstract

The Ordos Basin is one of the largest natural gas provinces in China. However, the origin of the gas produced from the Ordovician reservoirs remains puzzling. In order to determine the origin of the Ordovician weathered crust gas in Central Ordos gas field, we analyzed and collated chemical and isotopic data of produced gases along with fluid inclusion homogenization temperatures (HTs), and chemical and isotopic compositions. The weathered crust gas has methane $\delta^{13}C_1$ similar to the gas derived from Carboniferous–Permian (C–P) coal measures, ethane $\delta^{13}C_2$ close to the gas in the Ordovician reservoirs below salt (exclusively from Ordovician source rock) in the basin and is the driest gas among all the gases. In contrast to the thermogenic gas model, the gas shows a negative relationship of $\delta^{13}C_2$ to both the $\delta^{13}C_1$ and the dryness coefficient. Thus, a hypothesis is proposed that one end-member gas dominated by methane with less negative $\delta^{13}C_1$ and $\delta D_{methane}$ but more negative $\delta^{13}C_2$ has mixed with the other end-member with much less methane and less negative $\delta^{13}C_2$. The former represents late emplaced gas, likely from post-mature Ordovician sapropelic organic matter with $\delta^{13}C$ of $-27.8‰$. The other end-member gas representing less mature gas is derived from highly mature C–P coal measures with $\delta^{13}C$ of $-24.6‰$. Post genetic process — thermochemical sulphate reduction (TSR) in the Central Ordos gas field may have resulted in hydrocarbon gas becoming more dominated by methane with isotopically heavier carbon.

Keywords: Methane; H_2S, $\delta^{13}C$; δD; Thermochemical sulphate reduction; Ordos Basin

* Corresponding author. Tel.: +86 10 62007375; fax: +86 10 62010846.
E-mail address: Cai_cf@yahoo.com (C. Cai).

0920-4105/$ - see front matter © 2005 Elsevier B.V. All rights reserved.
doi:10.1016/j.petrol.2005.06.007

1. Introduction

The Ordos Basin (Fig. 1a) represents one of China's largest natural gas provinces with gas found in Ordovician and Carboniferous–Permian (C–P) strata, and oil produced from Triassic and Jurassic strata (Changqing, 1992). The Central Ordos gas field in this basin has gas reservoirs in the Ordovician close to the Carboniferous/Ordovician unconformity, thus is called weathered crust gas pools. The gas field has been proven to have reserves of 2384.85×10^8 m^3 (Xia, 2000). The Yulin and Suligemiao gas fields have gas reservoirs in the C–P reservoirs with reserves of about 4584.69×10^8 m^3 (Li et al., 2003).

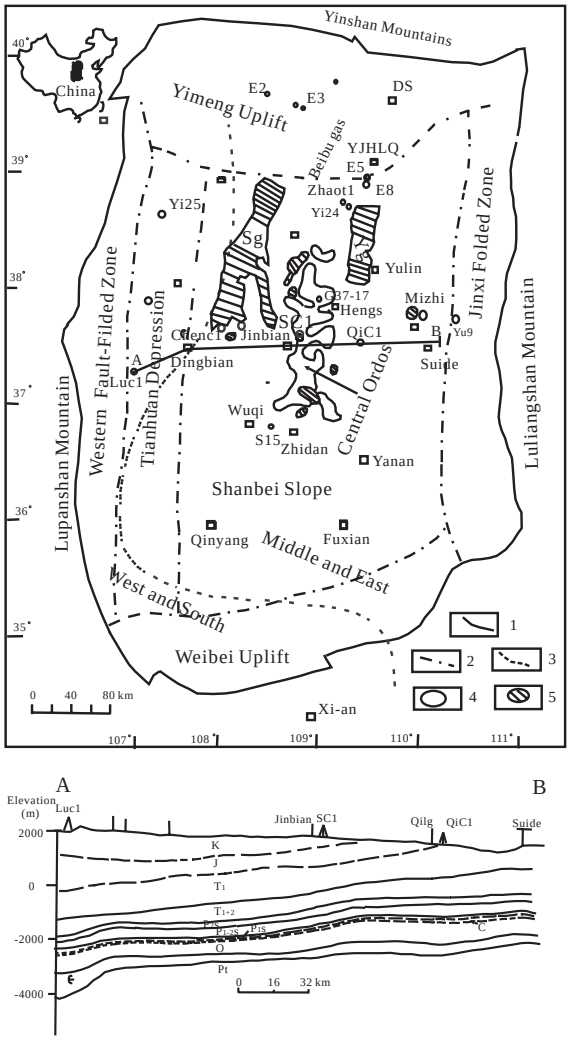

Fig. 1. Map showing geological tectonics and location of major petroleum exploration wells and gas fields in Paleozoic reservoirs (a), West–East cross section AB of Central Ordos (b). 1 Boundary of the basin; 2 Boundary of tectonic units; 3 Boundary of west-south and east-middle; 4 Gas field of the Ordovician reservoirs; 5 Gas fields of Carboniferous–Permian reservoirs; Yg represents Yulin Gas field and Sg is Suligemiao Gas field.

The majority of researchers agree that the gas in the Central Ordos gas field originated from mixing of Ordovician sapropelic (type I) to humic-sapropelic (type II_1) organic matter sourced gas with C–P coal sourced gas (e.g. Chen et al., 1993; Huang et al., 1996; Xia, 2000; Dai, 2000). But, there exists great debate about which source rock is the main precursor for the gas. This uncertainty is mainly due to poorly determined end-member gas. Based upon methane $\delta^{13}C_1$ and source rock TOC, the gas is interpreted mostly from C–P coal measures (e.g. Dai, 2000; Xia, 2000), however, upon evaluation of ethane $\delta^{13}C$ and methane δD, the gas appears more similar to the gas from type I kerogen in other Chinese basins (Chen et al., 1993; Xu and Sheng, 1996; Huang et al., 1996). Previous author explained relatively less negative $\delta^{13}C_1$ of the gas in the Ordovician weathered crust reservoirs as a result of segregative diffusion (Chen, 1994).

Hydrocarbon gas and non-hydrocarbon gas geochemistry have been used widely to understand the geological history of hydrocarbons and potentially as a management tool for production of gases (Kaufman et al., 1990). Present research has shown that organic matter types and their $\delta^{13}C$ (e.g. Behar et al., 1991; Berner and Faber, 1996) and organic matter maturity (Galimov, 1988; James, 1983; Schoell, 1980) control gas chemistry and carbon and hydrogen isotopic compositions. In Chinese basins, source rock types have been shown to be distinguished based mainly on the ethane $\delta^{13}C$ and methane δD values from different basins. That is, based upon case-studies, gas generated from type III kerogen is different from gas generated from type I and II_1 kerogen in that the former has ethane $\delta^{13}C$ less negative than $-28‰$ and methane δD typically more negative than $-190‰$ (e.g. Xu and Sheng, 1996; Chen et al., 2000; Song et al., 2004). In addition to source and maturity, post genetic processes such as mixing with biological methane, gas diffusion, source rock expulsion efficiency (Prinzhofer and Huc, 1995; Lorant et al., 1998; Prinzhofer et al., 2000), biological degradation (Coleman and Risatti, 1981;

Cai et al., 2002) and thermochemical sulphate reduction (e.g. Krouse et al., 1988; Cai et al., 2003 and 2004) can affect gas composition and isotopic signature to a great degree.

In this paper, we present evidence to show that organic matter types, their $\delta^{13}C$, maturity of the precursor organic matter (OM), and mixing of thermogenic gases from the C–P coal measures with gases sourced from the Ordovician type $I–II_1$ kerogen may have significant influence on chemistry and $\delta^{13}C$ of the natural gas produced from Ordovician weathered crust reservoirs. This conclusion is derived by comparing the gases produced from C–P reservoirs, from Ordovician weathered crust gas pools, and from Ordovician reservoirs below salt. Additionally, post genetic processes such as TSR rather than segregative diffusion may result in the gas becoming drier chemically and heavier isotopically within the reservoirs in the Central Ordos gas field.

2. Geological background

The Ordos Basin in the middle-west of China (Fig. 1a) is a large, intracratonic basin with an area of about 250,000 km^2. Its basement is Archeaean and Lower Proterozoic metamorphosed rock. Sitting above it is Middle and Upper Proterozoic terrestrial and marine clastics.

During the early Paleozoic, most of the Basin belonged to the passive continental margin. The Cambrian and Ordovician are dominated by platform facies carbonates. The upper part of the Upper Ordovician is found to be limited to the west-south of the Ordos Basin (Fig. 1a; Feng et al., 1994). From the end of the Ordovician to middle Carboniferous, the whole basin was uplifted and exposed to the surface (Figs. 1b and 2). Consequently, these strata experienced weathering and erosion, forming a 40–50 km wide weathered residue as the result of the Caledonian orogeny. Transgression occurred during the middle Carboniferous. The C–P sequence is composed of alternating marine and terrestrial coal-bearing detrital rock and bioclastics. The Triassic–Lower Cretaceous sequence is composed of lacustrine and fluvial clastic rocks that produce oil and coal. During the early Cretaceous, regional structure changed dramatically, the eastern part was uplifted and formed a westward gently sloping monocline (Fig. 1b). No sedimentation has taken place since the end of the early Cretaceous (Zhao et al., 1996 and references therein).

In the middle and east of the basin where Central Ordos gas field located, the Ordovician sequence from

System		Formation		Symbol	Thickness (m)	Lithology	Note
Permian	Upper	Shiqianfeng Fm		P_2S	150-300	Lacustrine facies sandstone and mudstone	C-P gas
		Upper Shihezi Fm		P_2sh	100-350		
	Lower	Lower Shihezi Fm		P_1x	20-220		
		Shangxi Fm		P_1s	20-140	Alternating marine and terrestrial sandstone, mudstone, coal and limestone	
Carb.	Upper	Taiyuan Fm		C_3t	50-400		
	Middle	Benxi Fm		C_2b	0-560		
Ordovician	Lower	Majiagou Fm	Member 5	O_1m^5	108-896	Platform carbontes with evaporites in Members 1,3 and 5	Weathered crust gas
			Member 4	O_1m^4			
			Member 3	O_1m^3			
			Member 2	O_1m^2			Gas below salt
			Member 1	O_1m^1			
		Liangjiashan Fm		O_1l	0-270		
		Yeli Fm		O_1y	0-150		

Fig. 2. Subdivision and stratigraphic nomenclature of the Ordovician–Permian section in the Central Ordos gas field with gas reservoirs shown.

the oldest to youngest (Fig. 2) includes: 1) Yeli Formation dolostone and dolomitic shale, 2) Liangjiashan Formation chert band-bearing dolostone and argillaceous dolostone, 3) Majiagou Formation. The Lower Ordovician Majiagou Formation is divided into five members, M1 to M5, beginning with the oldest formation (Fig. 2). The M2 and M4 sequences are dominated by open platform carbonates while the M1, M3 and M5 are dominated by evaporate platform anhydrite-bearing dolostone, anhydrite, and salt, and limited platform argillaceous dolostone and micrite. Anhydrite beds have been shown to occur only in the members M1, M3 and M5 with the thickest anhydrite found in the area around Well Yu9, Fuxian, Well S15, and in the Linfen area in the middle and east of the basin (Fig. 1a) (Feng et al., 1994).

3. Petroleum system

In the Ordos Basin, three types of natural gases have been found, including so called the weathered crust gas, the C–P gas and the gas below salt. The weathered crust gas is reservoired in anhydrite-bearing dolostone in Lower Ordovician Majiagou Formation Member 5 (M5 or O_1m_5) in Central Ordos gas field. The caprock for the weathered crust gas in the Central Ordos gas field is Middle Carboniferous Benxi Formation, which is comprised of 5 to 50 m thick bauxitic mudstone, coal, limestone, mudstone, shale and sandstone (Fig. 2). The bauxitic mudstone shows very low permeability values from 6.5×10^{-9} to 6.5×10^{-8} μm^2 (Ma et al., 1999), and it is found to occur in the most of the Central Ordos gas field. However, in some areas, the mudstone may be absent or be changed to sandstones and thus mixing of different sources of gas was proposed to occur there (Ma et al., 1999; Xia, 2000). The C–P gas is reservoired in Carboniferous–Permian sandstone in Suligemiao and Yulin gas fields. Small amount of the gas below salt was found in Wells E1, E5 and Yi24 in the north of the basin. The reservoirs for the gas below salt are located within Lower Ordovician Majiagou Formation Member 2 (M2, O_1m_2) below Member 3 salt and anhydrite beds. Their lithology is anhydrite-poor dolostone (Fig. 2) (Hui and Jia, 2001). The gas below salt is considered to be derived exclusively from Majiagou Formation source rock (Xia, 2000; Hui and Jia, 2001) (the reasons are explored in the following sections).

Potential source rocks for the Central Ordos gas field include C–P coal measures and Ordovician carbonates (Fig. 2). The Ordovician source rock is argillaceous dolostone, micrite and anhydrite-bearing carbonates with an algae-dominated marine amorphous sapropelic to humic-sapropelic organic matter (type I to II_1), and has vitrinite reflectance R_o values from 1.9 to 2.5% (i.e. post mature) (e.g. Chen et al., 1993). Total organic carbon (TOC) values are relatively low for the Ordovician (Table 1) after the potential source rock has been heated to R_o equivalent values >2.0%. The $\delta^{13}C$ values for the kerogen range from −28.2 to −26.4‰ with an average of −27.4 ± 0.5% ($n=13$) (Xia, 2000; Li et al., 2003).

The other possible source rock is C–P coal measures and limestone with R_o from 1.4% to 2.0% and relatively high TOC (Table 1). The coal and mudstone have humic type organic matter whilst the limestone is sapropelic-humic type (type II_2). The C–P coal and mudstone have kerogen $\delta^{13}C$ mainly from −25.5‰ to −23.1‰ with an average of −24.6‰ ($n=5$), and $\delta^{13}C$ of the C_{15}^{+} individual n-alkanes extracted from the organic matter from −28‰ to −24‰ (Zhang and Guan, 1997; Xia, 2000). The limestone has kerogen $\delta^{13}C$ of −26‰ and C_{15}^{+} individual n-alkanes $\delta^{13}C$ from −31‰ to −34‰ (Zhang and Guan, 1997). Chen (2002) argued against the limestone as the source of sapropelic "end member gas" for the weathered crust gas due to limited thickness and distance from the Central Ordos gas field. The gas in the C–P reservoirs is considered to be derived from the coal measures based upon gas geochemistry and the coal measures $\delta^{13}C$ and R_o data (e.g. Fu et al., 2003; Song et al., 2004).

4. Sample collection and analysis

The chemical compositions of the gas in the Central Ordos gas field were analyzed on HP6890 gas chromatograph with a precision of ±5 ppm. Gas dryness coefficient is expressed as molar $C_1/\sum C_{1-4}$ percentage with an error less than 0.004 mol% for all the analyzed gases (Table 2). Hydrocarbon gas $\delta^{13}C$ and δD isotope values were measured on a Finnigan MAT-252 mass spectrometer and are reported in δ

Table 1
Ordovician to Permian main petrology, source rock R_o, TOC and $\delta^{13}C$, and sulphur species in the sampled strata, and $\delta^{13}C_1$, $\delta^{13}C_2$, dryness coefficient in natural gases and interpreted source rock for the gases

Strata		Main petrology	Source rock			Gas geochemistry, sulphur species and source rock interpreted for the gases				
			R_o (%)	TOC[1] (%)	$\delta^{13}C$[1] (‰)	$C_1/\sum C_{1-4}$	$\delta^{13}C_1$	$\delta^{13}C_2$	Sulphur species	Source rock[3]
Carboniferous–Permian		Sandstone, mudstone and coal nipping limestone	1.4 to 2.0[1]	70.77 for coal[2]; 1.3 to 4.0 for dark mudstone[2, 3]; 0.81 to 0.95 for limestone[3]	>−25[2] or from −28 to −23 (−24.6 ± 2.0, n=5) [2] for coal and mudstone; −26 for limestone[3]	96.1 to 98.3/ 97.0 (12)	−34.2 to −30.0/ −32.2 (12)	−27.2 to −23.1/ −24.8 (12)	No significant H_2S and pyrite and no anhydrite	C–P[1–6]
Ordovician	Weathered crust	Carbonates, anhydrite and salt for the Ordovician	1.9 to 2.5[1,4]	0.09 to 1.49/0.31(32)[5]; 0.03 to 1.38/0.22[6] for the Ordovician	−28.2 to −26.4 (−27.8 ± 0.5, n=13)[2] for the Ordovician	99.1 to 99.9/ 99.6 (27)	−36.2 to −30.9/ −33.7 (19)	−33.1 to −23.7/ −28.6 (19)	Abundant anhydrite, widespread pyrite and up to 0.34% H_2S in gas composition in the reservoirs close to the unconformity	O and C–P[1–6]
	Below salt					90.0 to 94.2/ 92.1 (2)	−40.1 to −39.9/ −40.0 (2)	−32.7 to −29.1/ −30.9 (2)	No significant H_2S and pyrite in the reservoirs below salt	O[2, 5]

Data present as range/average (number); [1] From Chen et al. (1993); [2] from Xia (2000), [3] from Zhang and Guan, 1997; [4] from Huang et al. (1996); [5] from Hui and Jia (2001); [6] from Xu (1993).

Table 2
Chemistry and isotopic composition of natural gases in different reservoirs

Gas type	Gas field	Well	Reservoir	C_1	C_2	C_3	iC_4	nC_4	C_5+	CO_2	N_2	H_2S	$\delta^{13}C_1$	$\delta^{13}C_2$	$\delta^{13}C_3$	$\delta^{13}C_4$	δD_{C1}	$^3He/^4He$	$\delta^{34}S$–H_2S	$mC_1/\sum C_{1-4}$[1]
C–P gas	Yulin	Yu17-2	C–P	91.2	5.31	0.84	0.141	0.1351	0.15	–[2]	–	–	−34.2	−25.5	−23.1	−20.9	−191	=[3]	=	96.54
		Yu12	C–P	91.2	5.81	0.842	0.169	0.1647	0.24	–	–	–	−34.2	−26.3	−24.0	−23.1	−178	=	=	96.22
		S215	C–P	93.6	3.79	0.551	0.076	0.0807	0.08	0.76	0.86	–	−30.0	−25.8	−24.4	−23.1	−193	=	=	97.61
		S117	C–P	92.6	3.99	0.634	0.102	0.1105	0.15	1.51	0.71	–	−32.2	−26.0	−24.9	−23.8	−197	=	=	97.4
		Qi2	C–P	91.3	3.02	0.464	0.074	0.0724	0.09	2.67	1.90	–	−31.6	−25.2	−22.8	−21.4	−177	=	=	98.01
		Zhao4	C–P	90.7	5.46	1.087	0.205	0.2052	0.25	0.45	1.35	–	−31.3	−23.7	−23.0	−22.8	=	=	=	96.28
	Suligemiao	Tao6	C–P	93.4	2.76	0.36	0.039	0.0464	0.02	–	–	–	−30.0	−23.8	−25.4	−24.5	=	=	=	98.28
		Tao5	C–P	90.9	4.69	0.831	0.114	0.121	0.05	–	–	–	−33.9	−23.7	−24.2	−22.8	=	=	=	96.92
		Tao5	C–P	91	4.81	0.923	0.16	0.148	0.07	–	–	–	−33.5	−24.0	−24.7	−23.2	=	=	=	96.79
		Su6	C–P	87.3	5.44	1.13	0.171	0.17	0.07	–	–	–	−33.1	−23.6	−23.7	−22.5	=	=	=	96.21
		Su33-18	C–P	86.2	4.21	0.864	0.127	0.135	0.07	–	–	–	−31.7	−23.1	−23.4	−23.5	−190	=	=	97.0
		Su40-16	C–P	88.4	5.6	1.16	0.19	0.201	0.12	–	–	–	−30.2	−27.2	−25.5	−22.2	−198	=	=	96.12
Ordovician weathered crust gas	Central Ordos	SC1	O_1m_5	93.3	0.67	0.08	0.01	0.008	–	2.71	3.19	=	−33.9	−27.6	−26.0	−22.9	−169	2.1	=	99.58
		S5	O_1m_5	97.3	0.49	0.06	0.007	0.005	–	1.65	0.33	=	−33.8	−31.3	−27.1	=	−172	=	=	99.71
		S12	O_1m_5	96.8	0.78	0.1	0.01	0.01	–	1.65	0.63	0.019	−34.2	−25.5	−26.4	−20.7	−170	3.1	19.0	99.53
		S17	O_1m_5	93.9	0.72	0.08	0.01	0.01	0.01	4.55	0.62	0.057	−33.2	−30.8	−26.9	−22.2	−169	2.2	19.3	99.55
		S6	O_1m_5	92.6	0.32	0.03	0.001	0.002	0	4.86	2.22	0.338	−33.9	−30.1	−24.4	−24.4	=	3.3	16.3	99.8
		Zha2	O_1m_5	95.3	1.4	0.18	0.02	0.03	0.03	2.62	0.39	=	−35.2	−25.9	−25.4	−23.8	−175	=	=	99.13
		S33	O_1m_5	98.9	0.98	0.11	0.02	0.01	0.01	–	–	=	−34.0	−26.7	−25.5	−22.1	−172	=	=	99.42
		S34	O_1m_5	94.0	1.28	0.15	0.04	0.02	0.01	0.36	4.11	=	−35.3	−25.5	−24.4	−21.9	−177	=	=	99.20
		S45	O_1m_5	94.9	0.16	0.04	–	–	–	4.44	0.25	0.132	−33.5	−30.6	=	=	=	4.2	18.2	99.89
		S49	O_1m_5	94.6	0.31	0.03	0.001	0.001	–	4.52	0.47	=	−33.4	−31.8	=	=	−166	=	=	99.81
		S61	O_1m_5	97.5	0.77	0.10	0.007	0.008	–	1.61	–	=	−34.0	−27.7	−28.4	−24.8	−162	=	=	99.54
		S84	O_1m_5	93.0	0.81	0.12	0.01	0.01	0.02	5.09	0.99	=	−31.8	−28.5	−24.2	−20.9	−168	5.0	=	99.48
		S62	O_1m_5	96.6	0.54	0.07	0.005	0.006	–	2.15	0.64	=	−32.7	−33.1	−30.0	=	−171	4.1	=	99.67
		S30	O_1m_5	95.2	0.43	0.05	0.001	0.002	–	2.81	1.44	=	−32.8	−33.0	−25.0	=	−169	3.0	=	99.74
		S28	O_1m_5	96.0	0.74	0.09	0.01	0.009	–	2.84	0.25	=	−34.1	−28.3	−27.3	−24.1	−173	=	=	99.55
		S7	O_1m_5	93.7	1.28	0.17	0.03	0.03	0.02	4.67	0.15	=	−36.2	−23.7	−23.5	−21.5	−167	3.2	=	99.19
		S78	O_1m_5	95.5	0.91	0.11	0.01	0.01	0.01	2.22	1.23	=	=	=	=	=	=	=	=	99.44
		S77	O_1m_5	96.6	0.68	0.08	0.006	0.008	–	1.90	0.7	=	=	=	=	=	=	=	=	99.59
		S74	O_1m_5	95.8	0.88	0.15	0.03	0.02	0.01	2.55	0.32	=	=	=	=	=	=	3.6	=	99.44
		S91	O_1m_5	95.8	0.73	0.11	0.007	0.009	–	1.50	1.85	=	=	=	=	=	=	=	=	99.55
		S181	O_1m_5	95.7	0.21	0.03	0.001	0.002	–	2.69	1.39	=	=	=	=	=	=	4.7	=	99.87
		S88	O_1m_5	94.0	0.7	0.09	0.01	0.009	0.01	1.76	3.37	=	=	=	=	=	=	=	=	99.56
		Zha5	O_1m_5	95.9	0.75	0.09	0.01	0.009	0.01	3.00	0.2	=	=	=	=	=	=	=	=	99.54
		S57	O_1m_5	94.1	0.66	0.07	0.007	0.007	0.01	4.33	0.8	=	=	=	=	=	=	4.4	=	99.59
		Lin2	O_1m_5	98.1	0.74	0.10	0.02	0.01	–	0.40	0.47	0.003	−35.2	−25.9	−25.4	=	−176	=	17.9	99.54
		S24	O_1m_5	94.2	0.53	0.10	0.01	0.01	–	3.39	1.81	0.287	−32.5	−28.8	−26.4	=	−155	=	18.2	99.66
Gas below salt	Beibu	E1	O_1m_2-bs[4]	80.0	11.57	4.1	2.08	0.94	0.84	–	–	–	−40.1	−32.7	=	=	=	=	=	89.98
		Yi24	O_1-bs	86.5	7.28	2.19	0.72	0.66	0.88	–	–	–	−39.9	−29.1	=	=	=	=	=	94.17

Chemical compositions present in volume percentage, C_1 represents methane, δ^{13} C and in δD in ‰ relative to PDB and SMOW standard, respectively; $^3He/^4$ He in 10^{-8} , [1] in mol% with a maximal error of ± 0.004 mol%; [2] – represents <detection limit; [3] = represents no measurement; [4] -bs represents Ordovician reservoirs below salt.

notion in per mil (‰) relative to the Peedee Belemnite (PDB) marine carbonate standard and standard mean ocean water (SMOW), respectively. Their standard deviations are ±0.1 to 0.3‰ and ±1 to 2‰, respectively. The chemistry and isotopes of the C–P gas from Yulin and Suligemiao gas fields and the gas below salt in the Beibu area were collated from Fu et al. (2003) and Hui and Jia (2001), respectively. The method for $\delta^{34}S$ analysis of H_2S, pyrite and anhydrite can be found in Cai et al. (2001). The values are reported relative to the V-CDT standard with a standard deviation of ±0.2‰ and accuracy and precision of ±0.1‰ to 0.3‰ for the procedure. $^3He/^4He$ data were collected from material published by Liu et al. (2002).

Microthermometric measurements of fluid inclusions were made on calcite/dolomite/fluorite cements as well as on healed or semi-healed microfractures using a FLUID INC company U.S.G.S. Gas heating–cooling stage with a precision of ±1 °C. Measurements were made in strictly increasing temperature order so as to minimize inclusion re-equilibration. Chemical composition of gaseous fluid inclusions was quantitatively analyzed using a J-Y company RAMNOR U1000 laser laman probe according to the method of Pasteris et al. (1988) and Burke (2001).

The $\delta^{13}C$ values of hydrocarbon gas and CO_2 in inclusions were collated from Chen and Hu (2002) in which the gases were collected using vacuum ball grinding and then were measured for $\delta^{13}C$ on Delta S equipment with a standard deviation of ±0.3‰.

5. Results

5.1. Gas chemistry

In the Central Ordos gas field with gas reservoirs in Ordovician weathered crust, natural gas was measured to have hydrocarbon gases from methane to pentane and non-hydrocarbon gases including CO_2, N_2, H_2S (Table 2) and trace amounts of H_2, He and Ar. The gas is dominated by methane with a dryness coefficient (molar $C_1/\sum C_{1-4}$) > 99% and is drier than both the gas from C–P reservoirs (C–P gas) and the gas from Ordovician reservoirs below salt (gas below salt) (Table 1). In order to compare the gases, we normalized all ten parameters (C_1/C_2, C_2/C_3, dryness coefficient, $\delta^{13}C_1$, $\delta^{13}C_2$, $\delta^{13}C_3$, $\delta^{13}C_4$, $\delta^{13}C_2-\delta^{13}C_1$, $\delta^{13}C_3-\delta^{13}C_2$, δD_{C1}) using the method reported by Prinzhofer et al. (2000):

$$X_i = \left(R^i - R^i_{mean}\right)/\sigma^i$$

where R^i, R^i_{mean} and σ^i represent the absolute value, mean value and standard derivation of chemical or isotopic composition of the component i. The normalized value is plot on the Gastar diagram with the same scale (Fig. 3). From Fig. 3, the gas in the Central Ordos gas field has been shown to have the highest dryness coefficient values, C_1/C_2 and C_2/C_3 ratios among all the gases.

Relationship between $\ln(C_1/C_2)$ and $\ln(C_2/C_3)$ (Fig. 4a) shows a small variation in $\ln(C_2/C_3)$ relatively to $\ln(C_1/C_2)$ for both the C–P gas and the gas from weathered crust.

The natural gas in the Central Ordos gas field contains significant amounts of H_2S (up to 0.34%) (Table 2) while less than 4 ppm H_2S was reported in the C–P gas (Chen, 1994; Xia, 2000) and the gas below salt (Hui and Jia, 2001). The gas with relatively high H_2S concentration is shown to have relatively high CO_2 (Table 2), as is similar to the cases of Central Tarim and Sichuan Basin (Cai et al., 2001, 2003 and 2004). H_2S molar percentage among hydrocarbon gases $[100 \times H_2S/(H_2S + \sum C_{1-4})]$ has been used to indicate the degree of sulphate reduction (Worden et al., 1996; Cai et al., 2003). The H_2S percentages range from 0.001% to 0.17% and show a positive relationship to the dryness coefficient values (Fig. 4b), indicating that enhanced sulphate reduction has led to a more methane-dominated gas.

5.2. Isotopic composition of the natural gases

In the Ordovician weathered crust gas pools, the gas has similar $^3He/^4He$ ratio from 2.1 to 5.0×10^{-8} ($n = 19$). The $\delta^{13}C$ ranges for methane ($\delta^{13}C_1$) are −36.2‰ to −31.8‰; for ethane ($\delta^{13}C_2$) they are −33.1‰ to −23.7‰; for propane ($\delta^{13}C_3$) they are −30.0‰ to −23.5‰; and finally for butane ($\delta^{13}C_4$) they are −24.8‰ to −20.7‰ (Tables 1 and 2). The $\delta^{13}C_1$ and $\delta^{13}C_4$ values are similar to those of the C–P gas from −34.2‰ to −30.0‰ and from −24.5‰ to −20.9‰, respectively; but the $\delta^{13}C_1$ are significantly less negative than those of the gas below salt from −40.1‰ to −39.9‰. In contrast, the $\delta^{13}C_2$ values range widely from a more negative value than the gas

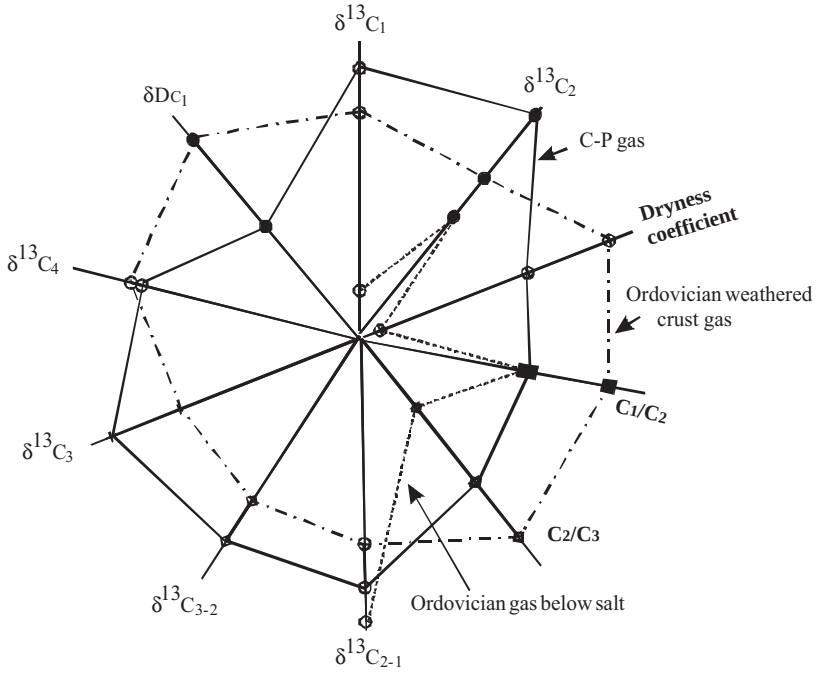

Fig. 3. Normalized Gastar diagram for natural gases from C–P reservoirs, Ordovician weathered crust reservoirs and Ordovician reservoirs below salt showing difference in the parameters using the method of Prinzhofer et al. (2000). All the axis are in the same scale.

below salt to the heaviest value of the C–P gas (Figs. 4c and 3). The gas from the weathered crust reservoirs shows a roughly negative relationship between $\delta^{13}C_1$ and $\delta^{13}C_2$ (Fig. 4c). The relationship is seldom observed in other case studies. The Ordovician weathered crust gas is shown to have the methane δD values (δD_{C1}) ranging from −177‰ to −155‰. The values are significantly less negative than those of the C–P gas from −198‰ to −177‰ (Table 2, Fig. 4d), and shows a wide range in $\delta^{13}C_1 - \delta^{13}C_2$ and large variation in $\delta^{13}C_2 - \delta^{13}C_3$ relative to the C–P gas (Fig. 4e and f).

When data from the weathered crust gas are plotted on the $\ln(C_i/C_j)$ vs. $(\delta^{13}C_i - \delta^{13}C_j)$ diagrams (Prinzhofer and Huc, 1995), the dots show trends of $\delta^{13}C_2$ becoming closer to $\delta^{13}C_1$ with rise in $\ln(C_1/C_2)$ (Fig. 4e), and small variation in $\ln(C_2/C_3)$ relative to $(\delta^{13}C_2 - \delta^{13}C_3)$ (Fig. 4f). The $\delta^{13}C_2$ becoming closer to $\delta^{13}C_1$ with the maturity is similar to other case studies previously reported by Schoell (1980) and James (1983), but different from that of experimental simulation under the closed-system (Lorant et al., 1998; Prinzhofer et al., 2000).

The plot of $(\delta^{13}C_{\text{alkane gases}} - \delta^{13}C_{\text{kerogen}})$ vs. carbon number was proposed by Clayton (2001), based on a Rayleigh fractionation model, to identify if a gas is a mixture from different sources. If a gas is derived from a single source, the gas is expected to show parallel relationship and follows the predicated trend in $\delta^{13}C$ from methane to butane. When we plot the data of the weathered crust gas on the diagram (Clayton, 2001), some of the gas shows $\delta^{13}C_1 > \delta^{13}C_2$ and/or $\delta^{13}C_3 > \delta^{13}C_2$; most of the gas shows methane and/or propane $\delta^{13}C$ derivation from the predicated trend of Clayton (2001) (Fig. 5). Significantly less negative $\delta^{13}C_1$ and more negative $\delta^{13}C_3$ than expected from the trend of Clayton (2001) indicates that the weathered crust gas is of mixing origin and altered by some secondary processes. The same conclusion can be made when the data are plotted on the natural gas plot of Chung et al. (1988) (not shown).

Relationships of dryness coefficient to $\delta^{13}C_2$ and methane δD (Fig. 4g and h) show that the weathered crust gas has ethane $\delta^{13}C$ becoming more negative with increasing dryness coefficient (correlation coef-

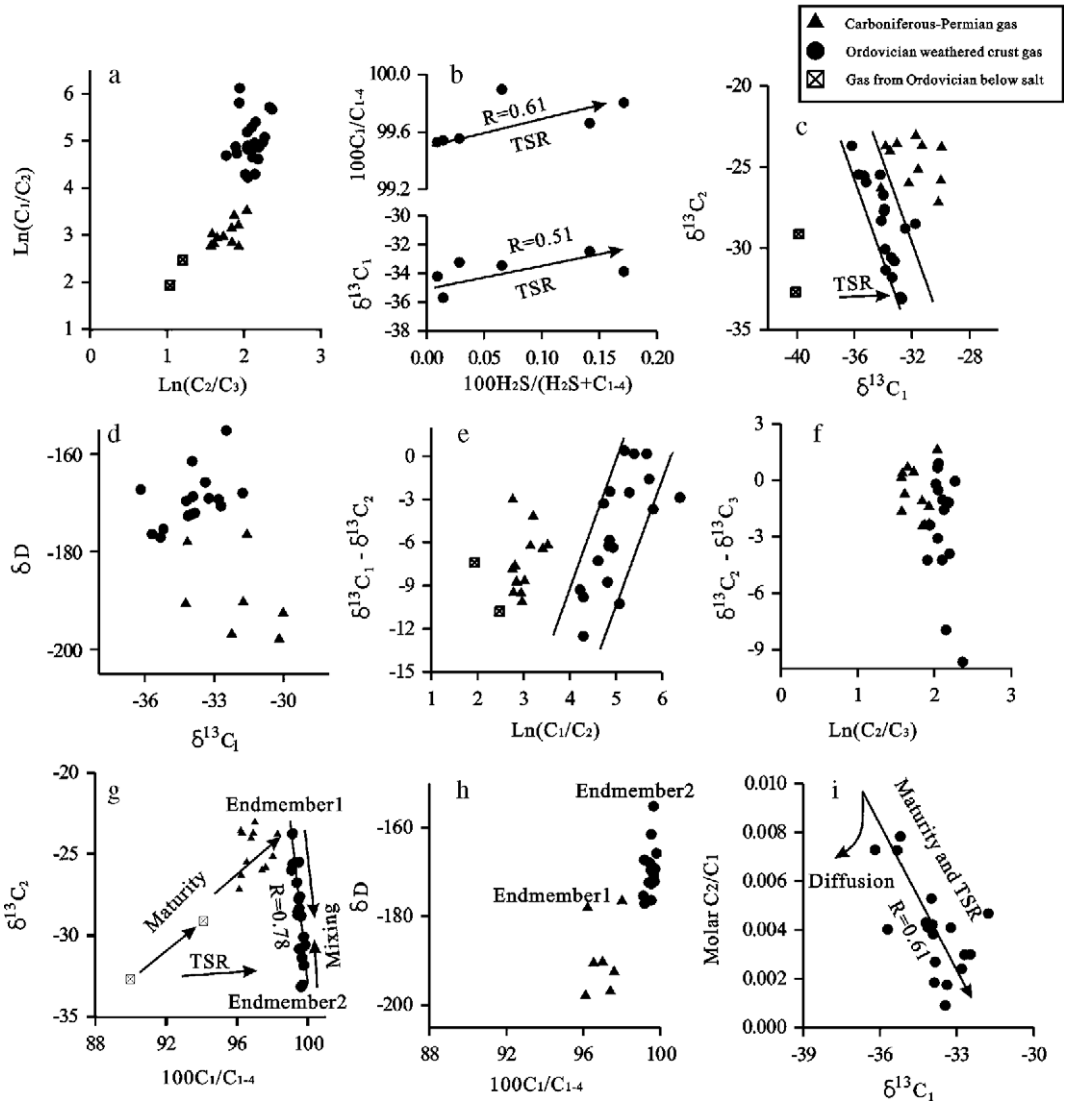

Fig. 4. Cross plots of (a) $\ln(C_1/C_2)$ vs. $\ln(C_2/C_3)$; (b) H_2S content among hydrocarbon gas vs. $\delta^{13}C_1$ and dryness coefficient; (c) $\delta^{13}C_1$ vs. $\delta^{13}C_2$; (d) $\delta^{13}C$ vs. δD of methane; (e) $\ln(C_1/C_2)$ vs. $(\delta^{13}C_1-\delta^{13}C_2)$; (f) $\ln(C_2/C_3)$ vs. $(\delta^{13}C_2-\delta^{13}C_3)$; (g) dryness coefficient vs. $\delta^{13}C_2$; (h) methane δD vs. dryness coefficient; (i) molar C_2/C_1 vs. $\delta^{13}C_1$ (see text for explanation).

ficient $R=0.78$). The weathered crust gas with the lowest dryness coefficient value has ethane $\delta^{13}C$ and methane δD close to the C–P gas.

Relationships of $\delta^{13}C_1$ to molar C_2/C_1 ratio and H_2S percentage (Fig. 4i and b) show that $\delta^{13}C_1$ becomes less negative with decreasing C_2/C_1 and increasing H_2S with a correlation coefficient value of 0.51 and 0.61, respectively. Because part of the H_2S may precipitate as pyrite, and C_2/C_1, and dryness coefficient values are influenced by mixing proportions of different gases, precursor organic matter maturity and TSR extent (see below sections), no high enough correlation coefficient values are expected. The H_2S has similar $\delta^{34}S$ values, ranging from +16.3‰ to +19.3‰ ($n=6$) (Table 2).

The CO_2 in a gas sample from Well SC1 has been measured to have $\delta^{13}C$ value of −15.7‰, indicating a significant contribution from organic matter.

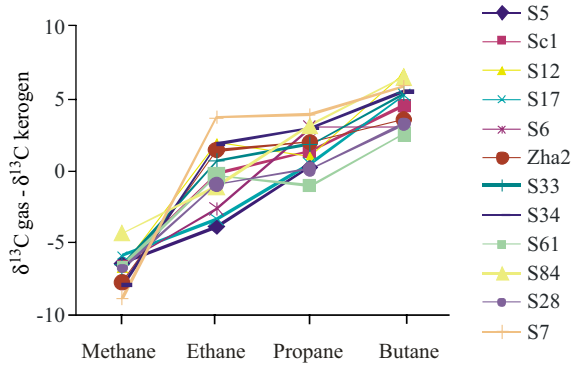

Fig. 5. Plot of carbon isotope ratio vs. hydrocarbon gas molecules from the gas produced from the weathered crust reservoirs (Clayton, 2001). These gas samples show cross-cutting relationships indicating the gas is of mixing origin. An average $\delta^{13}C$ value of Ordovician source rock (−27.8‰) is assumed as that of kerogen in the figure.

5.3. Fluid inclusions in Ordovician carbonates

Twenty-four limestone and dolostone samples from Ordovician Majiagou Formation from 12 wells in the Central Ordos gas field and 3 wells in the north of the basin have been carried out for fluid inclusion analyses. The fluid inclusions occur as congregative inclusions or in a string of beads in vug- or fissure-filling calcite cement, dolomite, and fluorite. The sizes of the fluid inclusions vary mostly from 3 to 10 μm with a maximum of 30 μm. All of the fluid inclusions are two-phase liquid-gas primary inclusions, with gas/liquid ratios mostly from 5% to 10%, up to 20%.

The analyses of inclusions in calcite cement show wide ranges for homogenization temperatures (HTs) from 60 to 220 °C (Fig. 6a). About 60% fluid inclusions have HTs greater than 130 °C. The fluid inclusion data suggests that there exist two episodes of calcite cementation reaching their peaks at 105 and 135 °C. A limited number of data show that saddle dolomite and fine crystalline dolomite has two peak HTs at 125 and 165 °C, respectively (Fig. 6b). The HTs measured in the dolomites in the study are similar to those reported in the same area by Feng et al. (1994). These authors observed that HTs range from 126 to 188 °C ($n=12$). In fluorite cement, the inclusions were measured to have two HT peaks from 135 °C and from 175 °C (not shown).

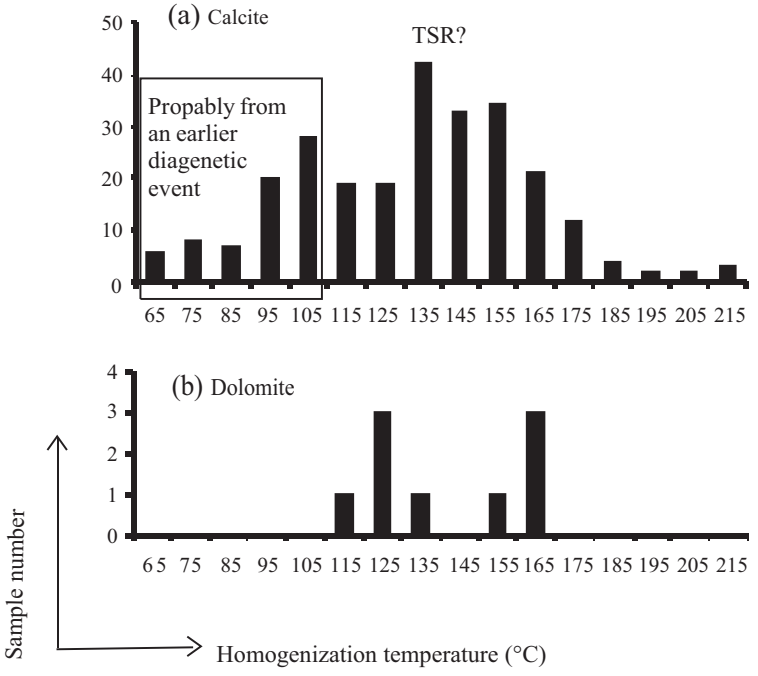

Fig. 6. Histogram showing homogenization temperatures in fluid inclusions in the cements in the Majiagou Formation carbonate rock: a) calcite, and b) dolomite.

Gaseous hydrocarbon inclusions in calcite cements were measured to have H_2O, alkane gas, H_2S, N_2, CO, and CO_2 components. The H_2S molar percentages range from 1.1 to 9.5% with an average of $4.8 \pm 3.8\%$ ($n=9$) (Table 3) whilst dissolved H_2S in liquid phase inclusions has concentrations from 3.0 to 9.5 mol% with an average of $5.1 \pm 2.0\%$ ($n=13$) in the study and up to 3.2 mol% measured by Liu et al. (2002). Feng et al. (1994) showed that H_2S in gas phase inclusions in saddle dolomite cement has concentrations from <detection limit to 17.5 mol% with an average of $7.7 \pm 7.6\%$ ($n=5$), while dissolved H_2S in five liquid phase inclusions has concentrations up to 15 mol% with an average of $8.2 \pm 7.5\%$ ($n=5$). Significantly higher H_2S concentrations in fluid inclusions than in gas samples may well indicate that high H_2S was generated previously and H_2S may have been precipitated as reduced sulphides such as pyrite, as supported by bedded authigenic pyrite on the top of the Majiagou Formation.

Five fluid inclusions in calcite cement have been analyzed for CO_2 $\delta^{13}C$ values and show the values ranging from −9.2‰ to −23.6‰ with an average of -12.4 ± 6.3‰ ($n=5$) (Table 4; Chen and Hu, 2002). Gas-liquid double phase saline inclusions coexisting with the inclusions were measured to have HTs >132 °C.

5.4. Paragenetic sequence and mineral isotopic ratios

The main diagenetic events in the Ordovician Majiagou Formation carbonates during burial include gypsum dehydration to form anhydrite, early diagenetic calcite cementation, mixed water dolomitization, calcite and salt dissolution, saddle dolomite cementation, late calcite cementation, anhydrite replacement by calcite (Yang et al., 1990; Feng et al., 1994; Shi and Luo, 1996) and pyrite and fluorite cementation (Fig. 7). Calcite dissolution was observed along stylolites and fractures to form vugs and enlarged fractures (Yang et al., 1990).

Calcite has, at some localities, completely replaced anhydrite and is present as pseudomorphs after anhydrite (e.g. Yang et al., 1990; Feng et al., 1994; Shi and Luo, 1996). In this study, we observed anhydrite replacement by calcite in finely crystalline dolostone in Wells S186 and G37-17 and at the depth of 3268.67 m in Well S156 in the Central Ordos gas field (not shown). The replacement has taken place at >109 °C, mostly >119 °C, as indicated by homogenization temperatures measured on fluid

Table 3
Chemistry of gas-phase inclusions of late calcite of Majiagou Formation carbonates

Well	Depth	H_2O	CH_4	C_2+	H_2S	N_2	CO	CO_2	SO_2
S188*	2502.2	17.1	61.7	5.1	1.2	5.7	4.0	5.22	–
Sheng4*	2313	15.2	49.2	6.8	1.6	11	8.2	7.82	–
Sheng4*	2313	15.4	56.2	5.3	1.1	5.3	3.7	13.1	–
S156*	3266.32	–	4.2	26.3	2.3	–	–	54.6	12.6
S47**	3174.17	–	14.2	3.9	9.1	–	–	72.8	–
S53**	3648	–	12.4	23.8	9.5	–	–	54.3	–
S53**	3649.85	–	10.3	8.3	9.1	6.2	–	66.1	–
S56**	3830.85	–	8.3	23.3	2.4	–	–	55.8	10.2
SC1**	3094.43	–	12.9	20	7.1	8.2	–	51.8	–

–represents <detection limit; *from this study; **from Liu et al. (2002).

Table 4
Isotopic composition of gas-phase inclusions of late calcite of Majiagou Formation carbonates

Well	Depth	$\delta^{13}C_1$	$\delta^{13}C_2$	$\delta^{13}C_3$	$\delta^{13}C_{CO2}$
S26	3534	−43.6	−23	−24	−9.3
S54	4102	−33.3	−26	−26	−9.5
S99	3602	−26.7	−25	=	−9.2
Sheng8	2289	−41.1	−23	−21	−10.2
Sc1	3666	=	=	=	−23.6

= represents no measurement.

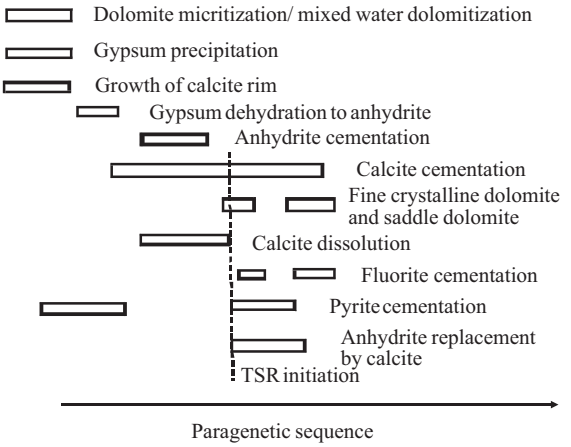

Fig. 7. Synthetic paragenetic sequence showing main stages in the diagenetic evolution of Majiagou Formation carbonates. Thermochemical sulphate reduction by hydrocarbon gases is indicated by replacement of anhydrite by calcite and gas chemistry and isotopic composition (see Fig. 4).

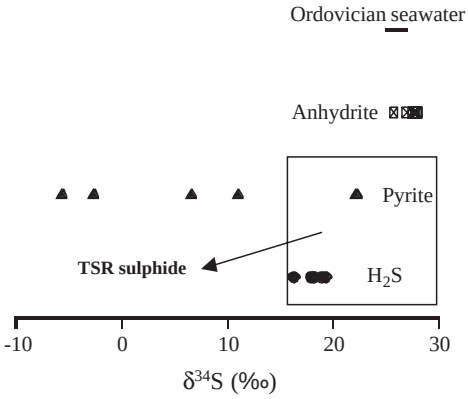

Fig. 8. Distribution of $\delta^{34}S$ of anhydrite, pyrite and H_2S gas from the Majiagou Formation. The H_2S and late diagenetic pyrite have relatively high and similar values indicating the sulphur were derived from Majiaguo Formation anhydrite.

inclusions of replacement calcite from 109 to 142 °C (123 ± 14 °C, $n=4$). Authigenic pyrite occurs in various forms, including in dispersive, and cubic habits and distributes along fractures or bed planes, indicating multi-stage precipitation. Authigenic, cubic pyrite bed was found on the top of Ordovician Majiagou Formation at some localities in the Central Ordos gas field with thickness from 10 to 50 cm (Xia, 2000).

Late diagenetic cubic pyrite in one sample from Well Chenc1 has $\delta^{34}S$ value of +22.2‰, close to those of coexisting H_2S (Fig. 8). The isotopic values for vug-filling authigenic pyrite in the Ordovician dolostones from Well S42 are from +6.6 to +11.0‰ ($n=2$), and they are from −5.7‰ to −2.6‰ ($n=2$) for pyrite in fractures and dispersive pyrite (Li et al., 2002). Ordovician anhydrite has $\delta^{34}S$ values from +25.8‰ and +28.0‰ with a mean value of +27.5 ± 0.7‰ ($n=8$) (Li et al., 2002). The values are slightly heavier than those of the H_2S and the highest $\delta^{34}S$ value of pyrite (Fig. 8).

5.5. Rebuilding of burial and geothermal history

The burial and geothermal history of the Well SC1 was reconstructed by running PRA Basinmod1 software based upon R_o and fluid inclusion homogenization temperatures (HTs). The result (Fig. 9) shows that rapid sedimentation took place during the early

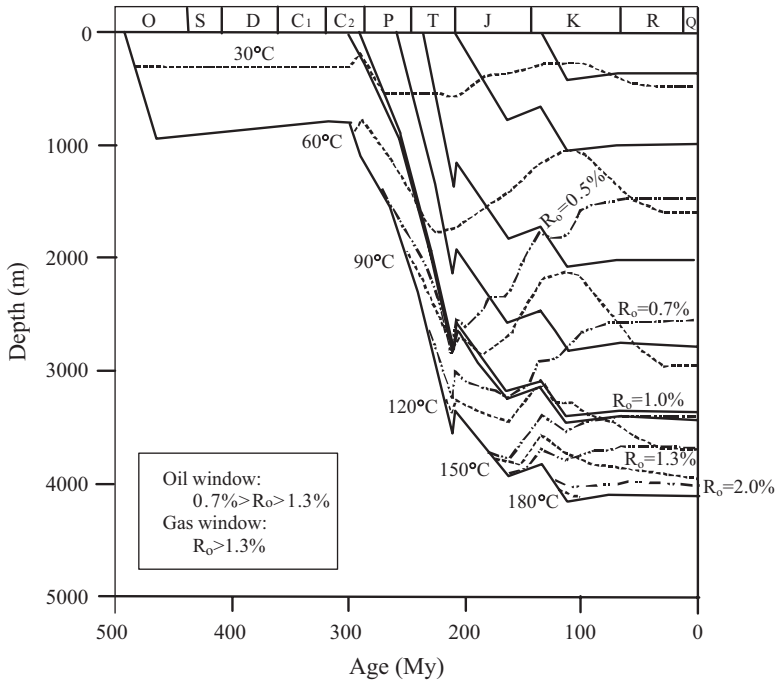

Fig. 9. Diagram showing a burial history constructed from Well SC1. Isotherms are constrained by vitrinite reflectance and fluid inclusion measurements.

Ordovician, late Carboniferous through to the middle Jurassic and early Cretaceous. Significant uplift occurred during the late Ordovician to early Carboniferous, middle Jurassic and late Cretaceous to Neogene with hundreds of meters eroded (Fig. 9). The strata experienced maximum burial and heating at the end of late Cretaceous. The maturation of sedimentary organic matter in the basin was influenced by various events. The Ordovician and C–P source rocks began generating oil during the late Triassic and early Jurassic, respectively and were buried further during the Jurassic and early Cretaceous. During the Yanshan movement during the early Cretaceous, a thermal event took place (Ren et al., 1994; Zhao et al., 1996) and led to peak gas generation from both the Ordovician algal organic matter and C–P coal measures. Based on apatite fission track, Zhao et al. (1996) and Ren et al. (1994) have proposed that cooling took place prior to at least 20 to 23 Ma due to rapid uplift and erosion in response to the rise of the Qinghai–Tibet plateau. The rise of the Qinghai–Tibet plateau is associated with the Asia–India collision and Himalayan orogeny.

6. Discussion

6.1. Origin of hydrocarbon gas

6.1.1. Kerogen- or oil-cracking gas?

Recent research by Behar et al. (1991), Prinzhofer and Huc (1995) and Lorant et al. (1998) has shown that methane, ethane and propane ratios along with differences in their isotopic composition can be used to distinguish kerogen-cracking gas from oil-cracking derived gas.

Behar et al. (1991) carried out closed-system pyrolysis and showed that during primary cracking, C_2/C_3 is almost constant while it increases significantly during the secondary cracking of oils. In contrast, the ratio of C_1/C_2 increases progressively during primary cracking and is then almost constant during secondary cracking. When isotopic data were considered, Prinzhofer and Huc (1995) and Lorant et al. (1998) concluded, based upon a case study from Angola, California and Kansas gas and experimental simulation, that a larger difference in $\delta^{13}C_2-\delta^{13}C_3$ than in C_2/C_3 results from primary cracking of kerogen whereas a larger difference in C_2/C_3 than in $\delta^{13}C_2-\delta^{13}C_3$ indicates secondary cracking of oil.

In the case of the Central Ordos gas field, the relationship between the ratios $\ln(C_2/C_3)$ versus $\ln(C_1/C_2)$ (Fig. 4a) shows a relatively constant ratio for C_1/C_2 relative to C_2/C_3. On the other hand, most of the gas has a small variation in $\ln(C_2/C_3)$ relative to $(\delta^{13}C_2-\delta^{13}C_3)$ difference (Fig. 4f), and $\delta^{13}C_1$ becomes closer to $\delta^{13}C_2$ as $\ln(C_1/C_2)$ values increase. These features are similar to a kerogen-cracking derived gas (Behar et al., 1991; Prinzhofer and Huc, 1995; Lorant et al., 1998), suggesting that the gas in the Central Ordos gas field is derived mainly from kerogen cracking directly.

However, occurrence of earlier emplaced oil in the reservoirs has been indicated by liquid hydrocarbon inclusions in some of the calcite cements. If the gas in the Central Ordos gas field was derived from cracking of the earlier emplaced oil, a great amount of pyrobitumen is expected to coexist with the gas (e.g. Cai et al., 1997). Unmatchably low amount of reservoir bitumen has been found (Li et al., 2003), further supporting our argument that the gas is mainly from kerogen cracking rather than from oil cracking. Earlier emplaced oil was found in fluid inclusions, however, neither oil pools nor significant amount of the oil cracking derived gas were found, thus, it is reasonable to consider that the earlier emplaced oil may have been lost prior to later gas emplacement.

6.1.2. Mixing of Ordovician source rock derived gas with C–P coal measures derived gas?

Methane $\delta^{13}C$ values of the gases in the weathered crust reservoirs are similar to those of the C–P gas. The feature does not mean that both the gases have the same source rock since there exist large differences in dryness coefficient and ethane $\delta^{13}C_2$ (Fig. 4g).

The roughly negative correlative relationship between molar C_2/C_1 and $\delta^{13}C_1$ (Fig. 4i) is well fit the thermogenic gas model (Galimov, 1988; James, 1983; Schoell, 1980). That is, under lower thermal stress, ^{12}C-kerogen is preferentially cracked as a result of kinetic isotope fractionation to generate relatively large molecules and isotopically light components due to their weaker bond strengths and thus leave the residual kerogen enriched in ^{13}C. Furthermore, with increasing maturity, a gas generated directly from kerogen is expected to be drier and isotopically hea-

vier. Ultimately, gas generated at very high maturities will have an isotopic composition close to that of the precursor kerogen. Based on the above, empirical equations between methane and $\%R_o$ and between ethane and $\%R_o$ have been established (e.g. Xu and Sheng, 1996). However, the negative relationships between $\delta^{13}C_1$ and $\delta^{13}C_2$ and between dryness coefficient and $\delta^{13}C_2$ (Fig. 4c and g) contradicting the model, instead, may well indicate that the weathered crust gas is a mixture of different sources. Similar conclusion has been made based on the alkane carbon number (n) and $\delta^{13}C_n$ plot of Clayton (2001) (Fig. 5). In Fig. 4g and h, the end-member1 is an intersection of both trend-lines of the C–P gas and of the weathered crust gas, and has the heaviest $\delta^{13}C_2$, lightest δD_{C1} and lowest dryness coefficient value among the weathered crust gas. The end-member1 may have been derived from highly mature humic organic matter, most likely from the C–P coal measures. In Chinese basins (Ordos Basin, Sichuan Basin and Tarim Basin), coal-derived gas has well been shown to have $\delta^{13}C_2$ less negative than −28‰ and δD_{C1} typically more negative than −190‰ (e.g. Chen et al., 1993; Xu and Sheng, 1996; Chen et al., 2000; Song et al., 2004) although the reason for the similarity is not clear. In the case of the study, all the C–P gas has $\delta^{13}C_2$ less negative than −28‰ and most of the gas has δD_{C1} more negative than −190‰, supporting that the C–P gas is derived from the coal measures (Fu et al., 2003; Song et al., 2004). The end-member1 has $\delta^{13}C_2$ and δD_{C1} values close to coal-derived gases in Chinese basins, supporting that it was generated from the C–P coal measures.

The other end-member (end-member2) is likely derived from type I kerogen from the Ordovician source rock, and *should* have similar chemical and isotopic composition to a gas from the same source rock. The gas below salt is most likely derived from the Ordovician source rock. This is based on the following lines of evidence: 1) no faults are found to cut both the Ordovician salt beds and the C–P strata; 2) salt and anhydrite beds serve as efficient barriers to block fluid flow; and 3) no source rocks have been found below the Ordovician (Hui and Jia, 2001). Thus, the end-member2 should have composition similar to the gas below salt. However, the gas below salt was found to have similar ethane $\delta^{13}C_2$ to the weathered crust gas, but shows much lower dryness coefficient and significantly more negative methane $\delta^{13}C_1$ than either the weathered crust gas, the C–P gas or the proposed end-member2, respectively (Table 2). That is, the gas below salt is totally not characteristic of the end-member2. Thus, it is proposed that the gas below salt and the end-member2 have the same source rock; but the end-member2 may have been generated at a higher maturity level than the gas below salt. However, the end-member2 has abnormally high dryness coefficient value (>99.8%) but unmatchably isotopically light ethane (close to the earlier emplaced gas), suggesting that it has been altered secondarily.

6.1.3. Secondary alteration of hydrocarbon gas

Secondary alteration processes reported to significantly change hydrocarbon gas chemistry and isotopic composition include segregative diffusion, biodegradation such as bacterial sulphate reduction (BSR) and thermochemical sulphate reduction (TSR) (e.g. Prinzhofer and Huc, 1995; Cai et al., 2002, 2003, 2004). Segregative diffusion or leakage has been reported to result in residual gas having relatively less negative $\delta^{13}C_1$ and increase in C_2/C_1, thus a concave upward shape will occur on the crossplot of $\delta^{13}C_1$ and C_2/C_1 (Prinzhofer et al., 2000). However, the gas from the weathered crust reservoirs does not show the feature (Fig. 4i), suggesting that leakage is not the main factor controlling evolution of the weathered crust gas. In addition, we have argued that the earlier-emplaced gas, if any, was escaped from the gas field and that later-stage gas was considered to have been generated mainly at the end of the early Cretaceous (Fig. 9). Since then, the temperatures of the reservoirs was too high (>100 °C; Fig. 9) for bacteria to survive, thus bacterial processes are unlikely to result in significant hydrocarbon gas secondary alteration.

In the below sections, we shall begin with discussing the origin of non-hydrocarbon gases (He and H_2S) in the weathered crust reservoirs, and show TSR leading to more methane-dominated gas with isotopically heavier carbon.

6.2. Mechanism of H_2S generation

Inert gas He can be used to reveal whether there has been a significant mantle-derived gas contributed

to the fluids in the basin. In the Ordos Basin, $^3He/^4He$ ratio ranges from 1.9 to 5.0×10^{-8}, giving no evidence of a mantle He contribution and indicating that the gas has been derived from sedimentary organic matter (Cai et al., 2001 and references therein).

Three mechanisms for H_2S generation in sedimentary basins have been proposed: 1) thermal decomposition of organic sulphur-containing petroleum and kerogen; 2) bacterial sulphate reduction (BSR) and 3) thermochemical sulphate reduction by hydrocarbons (TSR) (e.g. Orr, 1977; Machel et al., 1995; Worden et al., 1995; Worden and Smalley, 1996; Cai et al., 2001, 2002, 2003). Since we have argued against BSR as the source of hydrocarbon gas alteration, thus the H_2S may have organic sources or TSR.

6.2.1. Organic Sources of H_2S?

Small amount of H_2S may have been contributed from cracking of the kerogen at the temperature about 70 °C (Orr, 1977). However, the gas in the reservoirs below the salt show relatively low maturity and no significant H_2S, different from the weathered crust gas, suggesting even if early generated H_2S and hydrocarbon gas may have migrated to the weathered crust reservoirs but may well have been lost during the subsequent orogenies. Thus the H_2S in the reservoirs close to the unconformity was derived from sulphate reduction.

This is supported by the significantly different $\delta^{34}S$ values of the parent kerogen, and H_2S. The explanation follows. In general, organically derived H_2S is thought to have a $\delta^{34}S$ value close to or lower than parent S-enriched kerogen and oil (Orr, 1977; Cai et al., 2001, 2003). Marine kerogen contains sulphur that has a $\delta^{34}S$ value that is typically about 15‰ to 20‰ lower than the contemporary seawater. Thus, Ordovician kerogen and resulted organically derived H_2S should have a $\delta^{34}S$ of about +6‰ to +11‰ (Claypool et al., 1980). The value is significantly lower than the measured $\delta^{34}S$ values from the H_2S and late diagenetic pyrite, suggesting that the H_2S is not from decomposition of the kerogen.

6.2.2. Thermochemical Sulphate Reduction (TSR)

Because we have argued against an organic source for the sulphur in the H_2S, by elimination, thermochemical aqueous phase sulphate reduction is the likely origin of H_2S in the basin (e.g. Machel et al., 1995; Worden and Smalley, 1996):

$$SO_4^{2-} + \text{hydrocarbon} \rightarrow CO_3^{2-} + H_2S + \text{altered hydrocarbon} + H_2O$$

Anhydrite is typically replaced by calcite during sulphate reduction. Organically sourced CO_2 and inorganically sourced H_2S are the gas phase products of sulphate reduction reactions. However, at least some of the CO_2 is likely to react with aqueous calcium and magnesium from the anhydrite/dolomite source to produce solid phase calcite/dolomite. Similarly, H_2S will react with ferric minerals such as bauxitic mudstone capping the reservoirs or illite within carbonates to generate a great number of late diagenetic cubic pyrite. Thus, although the fluid inclusions contain 1.1 to 17.5 mol% H_2S, and bulk carbonates have reduced sulphur up to 6.2% (Hui and Jia, 2001), the concentration of H_2S in the natural gas is relatively low as compared with other TSR provinces (>5 mol% H_2S) in the Sichuan Basin, China (Cai et al., 2003, 2004) and other areas around the world (e.g. Krouse et al., 1988; Machel et al., 1995; Worden et al., 1995; Heydari, 1997). However, the H_2S distribution is similar to case-study in the Central Tarim and North Sea with <1% H_2S in the gas composition or dissolved water (Worden and Smalley, 2001; Cai et al., 2001). Consequently, the total amount of sulphide (reduced sulphur) generated by TSR or by BSR was proposed to be the best parameter to assess how much H_2S has been produced and thus to distinguish between BSR and TSR (Cai et al., 2001).

During natural TSR, there is commonly no significant sulphur isotope fractionation in the process of transformation of sulphate to sulphide or elemental sulphur (e.g. Orr, 1977; Machel et al., 1995; Cai et al., 2001) because dissolved sulphate may already have been totally reduced (Worden et al., 2000). In contrast, fractionation of about 20‰ was obtained during experimental TSR studies (Cross et al., 2004). In the Central Ordos gas field, the $\delta^{34}S$ values of the H_2S and late diagenetic pyrite range from +16.3‰ to +22.2‰. These values are slightly lower than those of Ordovician anhydrite that range from +25.8‰ and +28.0‰ ($n=8$) (Fig. 8), indicating 1) small fractionation during TSR in this case, or 2) mixing of TSR

derived H_2S with isotopically light H_2S derived from organic matter. In contrast, because those pyrite samples exhibit relatively low $\delta^{34}S$ values ranging from −6‰ to +11‰, they could have a complex origin involving both eogenetic BSR-related pyrite and later TSR (Fig. 8). This is similar to the case in Devonian Nisku Formation where the pyrite with $\delta^{34}S$ values from −35‰ to +20‰ was thought to be originated from both BSR and TSR (Riciputi et al., 1996). Pyrite of BSR origin was recently reported in the reservoirs in the Hetianhe gas field where meteoric water with sulphate reducing bacteria (SRB) flowed along the Carboniferous/Ordovician unconformity and SRB depleted both alkanes and organic acids and anions to generate reduced sulphur with very negative $\delta^{34}S$ values (Cai et al., 2002).

TSR is considered to be a thermodynamic phenomenon, but not a kinetic process (Heydari, 1997). The TSR initiation temperature is of significance in that it can be used to locate where TSR occurs and thus to predicate high H_2S distribution if the thermal and burial history of a basin has been rebuilt. The initiation temperature is generally thought to be greater than 120 to 140 °C (Sassen, 1988; Worden et al., 1995; Cai et al., 2001, 2003). In the case of the Ordos basin, fluid inclusion temperatures range from 60 to 220 °C. The lower temperature values (<105 °C) are probably from burial diagenetic calcite cementation that has nothing to do with TSR since replacement calcite after anhydrite has HTs mainly greater than 119 °C. TSR might have reached peak at 135 °C, the second peak temperature of calcite cement (Fig. 6b) although further work is required on these samples to ascertain this possibility. The TSR peak is consistent with other TSR studies (e.g. Cai et al., 2004).

6.2.3. Organic reactants involved in TSR

During sulphate reduction, liquid and gas phase petroleum have been reported to be involved in TSR (e.g. Orr, 1977; Krouse et al., 1988). In the case of Central Ordos gas field, oxidation of organic matter is well supported by the $\delta^{13}C$ values of CO_2 from the Well SC1 natural gas and fluid inclusions. The values are about −16‰ and as low as −23‰, respectively, which are much lighter than $\delta^{13}C$ of the bulk limestone from +0.18‰ to +1.40‰, thus suggesting a contribution from organic matter and perhaps mixing with previously existing inorganic CO_2 with $\delta^{13}C$ close to zero (e.g. Cai et al., 2001).

A positive shift in methane $\delta^{13}C$ with enhancing TSR (Fig. 4b) may be a consequence of kinetic isotope fractionation during methane oxidation (e.g. Cai et al., 2003, 2004). During TSR, ^{12}C-hydrocabon is expected to preferentially react with dissolved sulphates as a result of their weaker bond strengths (e.g. Krouse et al., 1988; Worden and Smalley, 1996). On the other hand, the weathered crust gas is shown to become drier as TSR proceeds (Fig. 4b). In many other TSR areas, the natural gases share the characteristics (e.g. Worden and Smalley, 1996; Cai et al., 2003, 2004). The patterns suggest that relatively high carbon number hydrocarbon molecules such as ethane and propane were involved in chemically reducing sulphate to sulphide. The reaction results in increased gas dryness values. The overall reactivity of ethane and propane involved in TSR were slightly greater than methane (e.g. Krouse et al., 1988). Once most of the heavy hydrocarbon molecules were exhausted by TSR, methane became heavily involved and underwent significant degrees of isotope fractionation. That is, TSR is likely induced by the earlier heavier hydrocarbon gas charge, but later dry gas charge was the dominant reducing agent involved in TSR (Cai et al., 2004; Worden and Smalley, 2004).

7. Conclusions

The gas in the weathered crust reservoirs is most likely derived from both Ordovician and C–P source rocks.

The H_2S in the weathered crust gas may have been generated by TSR. Subsequently, the H_2S could have reacted with Fe-bearing species to form 5 to 10 cm thick authigenic cubic pyrite bed on the top of Majiagou Formation.

TSR has altered the weathered crust gas chemically and isotopically, resulting in methane $\delta^{13}C$ values shift positively and increased dryness coefficient values.

In the Ordos Basin, methane δD and ethane $\delta^{13}C_2$ are altered by TSR to a lower degree than methane $\delta^{13}C_1$, and thus can be used to identify the source of the gas in the weathered crust reservoirs more efficiently.

Acknowledgements

The research is financially supported by China National Major Basic Development Program "973" (2003CB214605), FANEDD and China's National Natural Sciences Foundation (40173023).

References

Behar, F., Kressmann, S., Rudkiewicz, J.L., Vandenbroucke, M., 1991. Experimental simulation in a confined system and kinetic modelling of kerogen and oil cracking. Advance in Organic Geochemistry, vol. 19, pp. 173–189.

Berner, U., Faber, E., 1996. Empirical carbon isotope/maturity relationships for gases from algal kerogens and terrigenous organic matter, based on dry, open-system pyrolysis. Org. Geochem. 24, 947–955.

Burke, E.A., 2001. Raman microspectrometry of fluid inclusions. Lithos 55, 139–158.

Cai, C.F., Mei, B.W., Ma, T., Chen, C.P., Li, W., Liu, C.Q., 1997. Approach to Fluid–Rock Interaction in Tarim Basin. Geological Publishing House, Beijing. (in Chinese).

Cai, C.F., Hu, W.S., Worden, R.H., 2001. Thermochemical sulphate reduction in Cambro–Ordovician carbonates in Central Tarim. Mar. Pet. Geol. 18, 729–741.

Cai, C.F., Worden, R.H., Wang, Q.H., Xiang, T.S., Zhu, J.Q., Chu, X.L., 2002. Chemical and isotopic evidence for secondary alteration of natural gases in the Hetianhe Field, Bachu Uplift of the Tarim Basin. Org. Geochem. 43, 1415–1427.

Cai, C.F., Worden, R.H., Bottrell, S.H.., Wang, L.S., Yang, C.C., 2003. Thermochemical sulphate reduction and the generation of hydrogen sulphide and thiols (mercaptans) in Triassic carbonate reservoirs from the Sichuan Basin, China. Chem. Geol. 202, 39–57.

Cai, C.F., Xie, Z.Y., Worden, R.H., Hu, G.Y., Wang, L.S., He, H., 2004. Methane-dominated thermochemical sulphate reduction in the Triassic Feixianguan Formation East Sichuan Basin, China: towards prediction of fatal H_2S concentrations. Mar. Pet. Geol. 21, 1265–1279.

Changqing, 1992. Petroleum Geology of China vol 12—Changqing Oilfield. Petroleum Industry Press, Beijing. (in Chinese).

Chen, A.D., 1994. Origin and migration of natural gas in Ordovician reservoirs in Shan-gan-ning Basin Central gas field. Acta Petrolei Sinica 15 (2), 1–10 (in Chinese).

Chen, A.D., 2002. Feature of mixed gas in central gas fields of Ordos Basin. Pet. Explor. Dev. 29 (2), 33–38 (in Chinese).

Chen, M.J., Hu, G.Y., 2002. A new method in analysis of gas isotopes in fluid inclusion and the way of application. Pet. Explor. Dev. 23, 339–342.

Chen, A.D., Zhang, W., Xu, Y., 1993. Isotope characteristics and its application of products from hydrocarbon generating thermal simulation experiments on sedimentary rock. Sci. China Ser. B 23, 209–217 (in Chinese).

Chen, J.F., Xu, Y.C., Huang, D.F., 2000. Geochemical characteristics and origin of natural gas in Tarim Basin, China. Am. Assoc. Pet. Geol. Bull. 84, 591–606.

Chung, H.M., Gormly, J.R., Squires, R.M., 1988. Origin of gaseous hydrocarbons in subsurface environments. Theoretical considerations of carbon isotope distribution. Chem. Geol. 71, 97–104.

Claypool, G.E., Holser, W.T., Kaplan, I.R., Sakai, K., Zak, I., 1980. The age curves of sulfur and oxygen isotopes in marine sulfate and their mutual interpretation. Chem. Geol. 28, 199–260.

Clayton, C., 2001. Carbon isotope fractionation during natural gas generation from kerogen. Mar. Pet. Geol. 8, 232–240.

Coleman, D.D., Risatti, J.B., 1981. Fractionation of carbon and hydrogen isotopes by methane-oxidizing bacteria. Geochim. Cosmochim. Acta 5, 1033–1037.

Cross, M.M., Manning, D.A.C., Bottrell, S., Worden, R.H., 2004. Thermochemical sulphate reduction (TSR): experimental determination of reaction kinetics and implications of the observed reaction rates for petroleum reservoirs. Org. Geochem. 35, 393–404.

Dai, J.X., 2000. The study on gas source rock of Ordovician weathered crust natural gas reservoirs in Changqing Gas Field. In: Dai, J.X. (Ed.), The Geology and Geochemistry of Natural Gas, vol. 2. Petroleum Industry Press, Beijing, pp. 247–255 (in Chinese).

Feng, Z.Z., Bao, Z.D., Zhang, Y.S., Tan, J., 1994. Stratigraphy, Petrology and Lithofacies Paleogeography of Ordovician in Ordos Basin. Geological Press, Beijing. (in Chinese).

Fu, S.T., Feng, Q., Zhang, W.Z., 2003. Characteristics of the individual carbon isotope of natural gas from Suligemiao and Jianbian gas fields in Ordos Basin. Acta Sedimentologica Sinica 21 (3), 258–532 (in Chinese).

Galimov, E.M., 1988. Sources and mechanisms of formation of gaseous hydrocarbons in sedimentary rock. Chem. Geol. 71, 77–95.

Heydari, E., 1997. The role of burial diagenesis in hydrocarbon destruction and H_2S accumulation, Upper Jurassic Smackover Formation, Black Creek field, Mississippi. Am. Assoc. Pet. Geol. Bull. 81, 26–45.

Huang, D., Qiong, C.W., Yang, J.J., Xu, Z.Q., Wang, K.R., 1996. The source of the gas in large-scale Central gas field in the Ordos Basin. Chin. Sci. Bull. 41 (17), 1588–1592.

Hui, K.Y., Jia, H.C., 2001. Study on the source of natural gas in Ordovician in Tabamiao area of northern Ordos Basin. J. Min. Petrol. 21, 23–27 (in Chinese).

James, A.T., 1983. Correlation of natural gas by use of carbon isotopic distribution between hydrocarbon components. Am. Assoc. Pet. Geol. Bull. 67, 1176–1191.

Kaufman, R.L., Ahmed, A.S., Elsinger, R.J., 1990. Gas chromatography as a development and production tool for fingerprinting oils from individual reservoirs: application in the Gulf of Mexico. Gulf Coast Section, SEPM Foundation Ninth Annual Research Conference Proceedings, pp. 263–282.

Krouse, H.R., Viau, C.A., Eliuk, L.S., Ueda, A., Halas, S., 1988. Chemical and isotopic evidence of thermochemical sulfate reduction by light hydrocarbon gases in deep carbonate reservoirs. Nature 33, 415–419.

Li, J.F., Lan, F.X., Guo, J.M., 2002. Origin of H_2S from Ordovician reservoirs in Changqing Gas Field. In: Liang, D.G., Huang, D.F., Ma, X.H., Li, J.M. (Eds.), The 8th National Organic Geochemistry Proceedings. Petroleum Industry Press, Beijing, pp. 188–192 (in Chinese).

Li, J., Hu, G.Y., San, X.Q., Chen, M.J., Li, Z.S., Xie, Z.Y., Yan, Q.T., 2003. Research on oil and gas pool formation in the Ordos Basin (unpublished report). Lanfang Branch of Petroleum Exploration and Development Institute, Lanfang (in Chinese).

Liu, D.L., Tan, Y., Sun, X.R., Li, Z.S., Fang, G.Q., Tao, S.Z., 2002. Characteristics of Paleozoic fluid inclusions and their relationship with oil–gas evolution in Ordos Basin. Acta Sedimentologica Sinica 20, 695–704 (in Chinese).

Lorant, F., Prinzhofer, A., Behar, F., Huc, A.Y., 1998. Carbon isotopic and molecular constraints on the formation and the expulsion of thermogenic hydrocarbon gases. Chem. Geol. 147, 249–264.

Ma, Z.F., Zhou, S.X., Yu, Z.P., Pan, L.H., Wang, H.K., 1999. The weathered paleo-crust in the Ordovician in Ordos Basin and its relationship to gas accumulation. Pet. Explor. Dev. 26 (5), 21–23 (in Chinese).

Machel, H.G., Krouse, H.R., Sassen, R., 1995. Products and distinguishing criteria of bacterial and thermochemical sulfate reduction. Appl. Geochem. 8, 373–389.

Orr, W.L., 1977. Geologic and geochemical controls on the distribution of hydrogen sulfide in natural gas. In: Campos, R., Goni, J. (Eds.), Advances in Organic Geochemistry 1975. Pergamon Press, Oxford, pp. 571–597.

Pasteris, J.D., Wopenka, B., Seitz, J.C., 1988. Practical aspects of quantitative laser Raman microprobe spectroscopy for the study of fluid inclusions. Geochim. Cosmochim. Acta 52, 979–988.

Prinzhofer, A., Huc, A.Y., 1995. Genetic and post-genetic molecular and isotopic fractionations in natural gases. Chem. Geol. 126, 281–290.

Prinzhofer, A., Mello, M.R., Takaki, T., 2000. Geochemical characterization of natural gas: a physical multivariable approach and its applications in maturity and migration estimates. Am. Assoc. Pet. Geol. Bull. 84, 1152–1172.

Ren, Z.L., Zhao, Z.Y., Zhang, J., Yu, Z.P., 1994. Research on paleotemperature on the Ordos Basin. Acta Sedimentologica Sinica 12 (1), 56–65 (in Chinese).

Riciputi, L.R., Cole, D.R., Machel, H.G., 1996. Sulfide formation in reservoir carbonates of the Devonian Nisku Formation, Alberta, Canada: an ion microprobe study. Geochim. Cosmochim. Acta 60, 325–336.

Sassen, R., 1988. Geochemical and carbon isotopic studies of crude oil destruction, bitumen precipitation and sulfate reduction in the deep Smackover Formation. Org. Geochem. 12, 351–361.

Schoell, M., 1980. The hydrogen and carbon isotopic composition of methane from natural gases of various origins. Geochim. Cosmochim. Acta 44, 649–661.

Shi, F.Z., Luo, J.L., 1996. The diagenesis and characteristics of Lower Paleozoic carbonate reservoir in the Ordos Basin. Journal of Northwest University (Natural Science Edition) 26 (6), 526–532 (in Chinese).

Song, Y., Dai, J.X., Xia, X.Y., Qin, S.F., 2004. Genesis and distribution of natural gas in the foreland basins of China. J. Pet. Sci. Eng. 41, 21–29.

Worden, R.H., Smalley, P.C., 1996. H_2S-producing reactions in deep carbonate gas reservoirs: Khuff Formation Abu Dhabi. Chem. Geol. 133, 157–171.

Worden, R.H., Smalley, P.C., 2001. H_2S in North Sea oil fields: importance of thermochemical sulfate reduction in clastic reservoirs. In: Cidu, R. (Ed.), The Proceedings of the 10th International Symposium on Water–Rock Interaction, vol. 2. Balkema, Lisse, pp. 659–662.

Worden, R.H., Smalley, P.C., 2004. Does methane react during thermochemical sulfate reduction? Proof from the Khuff Formation, Abu Dhabu. In: Wanty, R., Seal, R.R. (Eds.), Water–Rock Interaction 2004. Taylor and Francis Group, London, pp. 1049–1053.

Worden, R.H., Smalley, P.C., Oxtoby, N.H., 1995. Gas souring by thermochemical sulfate reduction at 140 °C. Am. Assoc. Pet. Geol. Bull. 79, 854–863.

Worden, R.H., Smalley, P.C., Oxtoby, N.H., 1996. The effects of thermochemical sulfate reduction upon formation water salinity and oxygen isotopes in carbonate gas reservoirs. Geochim. Cosmochim. Acta 60, 3925–3931.

Worden, R.H., Smalley, P.C., Cross, M.M., 2000. The influence of rock fabric and mineralogy on thermochemical sulfate reduction: Khuff Formation, Abu Dhabi. J. Sediment. Res. 70, 1210–1221.

Xia, X.Y., 2000. Hydrocarbon potential evaluation of carbonates and gas source rock correction of Changqing gas field. Petroleum Industry Press, Beijing. (in Chinese).

Xu, Z.Q., 1993. Machemism of natural gas generation in the Ordovician in the Ordos Basin (internal report). Xi'an, Changqing Oil- and Gas-field company, pp. 20–120 (in Chinese).

Xu, Y.C., Sheng, P., 1996. A study of natural gas origins in China. Am. Assoc. Pet. Geol. Bull. 80, 1604–1626.

Yang, J.J., Pei, X.G., Zhang, J.S., Chen, A.D., Li, Y.D., 1990. The law of natural gas accumulation in the Ordos Basin. Key project of China's 7th Five Plan (code: 75-54-01-10). Changqing Oil and Gas Fields, Xi'an (in Chinese).

Zhang, W.Z., Guan, D.S., 1997. Carbon Isotope Geochemistry of Liquid Hydrocarbon Molecular Series. Petroleum Industry Press, Beijing. (in Chinese).

Zhao, M.W., Behr, H.J., Ahrendt, H., Wemmer, K., Ren, Z.L., Zhao, Z.Y., 1996. Thermal and tectonic history of the Ordos Basin, China: evidence from apatite fission track analysis, vitrinite reflectance, and K-Ar dating. Am. Assoc. Pet. Geol. Bull. 80, 1110–1134.